Quenching of the relaxation pathway in the Weyl semimetal TaAs

Liu, Jiayun; Cheng, Liang; Zhao, Daming; Chen, Xiaoxuan; Sun, Handong; Li, Zhilin; Wang, Xinbo; Zhu, Jian-Xin; Chia, Elbert E. M.

2020

Liu, J., Cheng, L., Zhao, D., Chen, X., Sun, H., Li, Z., Wang, X., Zhu, J. & Chia, E. E. M. (2020). Quenching of the relaxation pathway in the Weyl semimetal TaAs. Physical Review B, 102(6), 064307-1-064307-7. https://dx.doi.org/10.1103/PhysRevB.102.064307

https://hdl.handle.net/10356/151131

https://doi.org/10.1103/PhysRevB.102.064307

Quenching of relaxation pathway in Weyl semimetal TaAs

Jiayun Liu,[1] Liang Cheng,[1,2] Daming Zhao,[1] Xiaoxuan Chen,[1] Handong Sun,[1] Jian-Xin Zhu,[3] Zhilin Li,[4] Xinbo Wang,[4] and Elbert E. M. Chia[1,*]

[1] *Division of Physics and Applied Physics, School of Physical and Mathematical Sciences, Nanyang Technological University, 21 Nanyang Link, Singapore 637371*
[2] *State Key Laboratory of Electronic Thin Films and Integrated Devices University of Electronic Science and Technology of China Chengdu 610054, China*
[3] *Theoretical Division and Center for Integrated Nanotechnologies, Los Alamos National Laboratory, Los Alamos, New Mexico 87545, USA*
[4] *Beijing National Laboratory for Condensed Matter Physics, Institute of Physics, Chinese Academy of Sciences, Beijing 100190, China*

(Dated: June 3, 2021)

Since tantalum arsenide (TaAs) has been experimentally verified as a Weyl semimetal, intensive research has been devoted to study the unique properties of the material. Despite that, the ultrafast dynamics of TaAs is still not very well understood. In this work, we studied the relaxation dynamics in TaAs using transient reflection spectroscopy. From the transient reflection measurement, we observed either a single (fast) or dual (fast and slow) relaxation depending on the probing wavelength. The additional relaxation channel has been attributed to an asymmetric population of photoexcited electrons and holes.

I. INTRODUCTION

Topological insulators (TIs) are unique materials with insulating bulk states while having spin-polarized conducting surface states that are topologically protected [1–3]. Due to this unique electronic property, TIs have seen a plethora of applications like broadband photodetector [4–6], spin current injection [7, 8] and detection [9, 10]. Following the topological classification of materials, Dirac semimetal has been predicted theoretically [11] and has since been experimentally confirmed through mapping of the band structure by angle-resolved photoemission spectroscopy (ARPES) [12, 13]. These Dirac semimetal has gapless dispersion at certain points in momentum space known as Dirac points. These three-dimensional (3D) Dirac points have been experimentally observed in Cd_3As_2 [12] and BiO_2 [14] crystals. The states on these Dirac points are doubly-degenerate [15] which can be lifted if either the time reversal symmetry $\mathcal{T}$, or the inversion symmetry $\mathcal{I}$, is broken [16]. The breaking of either $\mathcal{T}$ or $\mathcal{I}$ results in the splitting of the Dirac point into a pair of Weyl nodes in momentum space [17]. This splitting leads to the formation of a Weyl semimetal which corresponds to a new topological phase with fascinating properties like topologically-protected Fermi arc states [18, 19] and chiral anomaly [20].

The Weyl nodes separated in momentum space each has a well-defined chirality of either $\chi = +1$ or $\chi = -1$ [21]. This well-defined chirality gives rise to chirality selection rule where right-circularly polarized light is able to excite electrons from the positive k side of the $\chi = +1$ Weyl cone but not the negative side, and vice versa. The energy to excite electrons from the valence band to the conduction band is different for electrons on the positive and the negative k side of the Weyl cone. Therefore, circular dichroism can be achieved in a Weyl semimetal through the selective excitation of electrons in the Weyl cones. Through the manipulation of circular dichroism, optical response in the mid-infrared regime has been experimentally demonstrated [22] in tantalum arsenide (TaAs), a type-I Weyl semimetal [23]. Exploiting the gapless dispersion in TaAs, further experiments have reported broad bandwidth response of TaAs from visible to the mid-infrared regime [24]. This wide spectral bandwidth of TaAs is ideally suited for application in optoelectronics.

The unique topological properties of TaAs may be the reason for the large second-order nonlinear susceptibility coefficient [25], that gives rise to physical observations like large second harmonic generation [26] and large photocurrent [27]. Besides the aforementioned properties, TaAs has large absorption coefficient [28] and high carrier mobility [29]. These properties are present independent of the thickness of TaAs since it is a 3D material unlike transitional metal dichalcogenides [30] and graphene [31] where the material properties are layer dependent. The combination of these properties has made TaAs a potential material for applications in high-sensitivity photodetector [24] and field-effect-transistors [32]. Despite the vast research interest, the transient dynamics of TaAs has not been well understood, with literature reporting different decay dynamics (single decay dynamics [33] and multiple decay dynamics [34]) for TaAs. However, knowledge of the transient dynamics is crucial since it determines the response time of the material which is especially important in ultrafast optoelectronics.

In this work, we studied the ultrafast response of TaAs in the optical regime through transient reflection spectroscopy with varying pump fluence. We noted two relaxation channels for the hot injected electrons in TaAs

* elbertchia@ntu.edu.sg

by the pump pulse. We attributed the fast decay to the electron-hole (e-h) recombination that occurs in the picosecond (ps) timescale. For the slower decay occuring in the tens of ps, we attribute it to carrier cooling via electron-phonon (e-ph) coupling.

II. METHOD

TaAs crystals were grown by chemical vapor transport (CVT) method using iodine as the transport agent. In a typical run, tantalum, arsenic and a small amount of iodine were loaded into a silica ampule. The ampule was evacuated, sealed and heated slowly to 1050°C and then put to a temperature gradient from 1030°C to 1070°C where the CVT proceeded for two weeks. TaAs then reacts with iodine at the cooler end, forming gaseous species, transported to the hotter end, and finally recrystallize into millimetre-sized TaAs single crystals. More details on the crystal growth can be found in [35].

The transient reflection (TR) spectroscopy is a pump-probe technique to probe excited-state dynamics. Our TR measurement is performed using HELIOS Fire (Ultrafast Systems LLC). A Ti:sapphire laser (Coherent Legend Elite) with central wavelength at 800 nm, pulse duration of 30 fs and repetition rate of 1 kHz was used as both the pump and generation of white light probe. The white light probe allows for the probing of electron filling at different k-points of the conduction band. The laser is split into two paths for TR spectroscopy. The white light probe pulse is generated by focusing the laser from one path onto a sapphire crystal. The co-polarized pump and probe pulse are focused on the TaAs sample with spot sizes of 115 μm and 100 μm respectively. The spectrum of the reflected probe pulse is measured at different pump probe delays. The normalized change in reflectance (ΔR/R) at different pump-probe delay was recorded and the TR spectra plotted. The absorption spectrum of TaAs is measured at room temperature with variable-angle spectroscopic ellipsometry (J.A. Woollam Co.).

III. RESULTS

The steady-state absorption spectra of the Weyl semimetal TaAs measured at room temperature is shown in Fig. 1. The two absorption peaks at 440 nm (2.82 eV) and 560 nm (2.21 eV) are consistent with calculated band structure reported in literature [28] where the 440 nm peak corresponds to transition from –0.2 eV to 2.6 eV at the N point, while the 560 nm peak corresponds to the transition from –1 eV to 1.1 eV at the Z point.

To probe the ultrafast dynamics of the Weyl semimetal in the visible regime, the TaAs is excited with 800 nm pump and probed from 430 nm to 720 nm at room temperature. The pseudo-color TR spectra plot of ΔR/R is displayed in Fig. 2. The spectra exhibits a positive ΔR/R

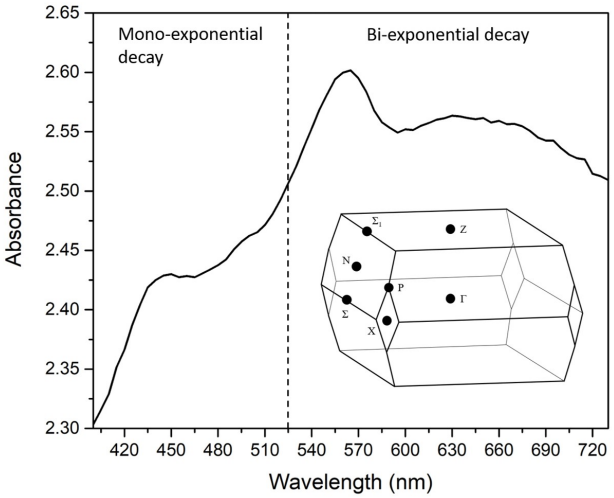

FIG. 1. Steady state absorption spectrum of TaAs measured by variable-angle spectroscopic ellipsometry at room temperature. Vertical dashed lines separate regions where TR probe can be fitted with mono/bi-exponential decay function. Absorption peaks at 440 nm and 560 nm corresponds to the transition at N and Z point respectively. Inset depicts the first Brillouin zone of TaAs

signal for probe wavelengths between 500 nm to 600 nm. The positive ΔR/R signal corresponds to the process of photobleaching (PB), where the states in the conduction band that were filed by valence-band electrons absorbing the pump pulse, cannot be filled anymore by a subsequent probe pulse. This results in a smaller absorption, and thus larger reflection, than without pump. For probe wavelengths outside this range, the TR signal is initially negative, and changes to positive within a ps timescale. The negative signal corresponds to photoinduced absorption (PIA), where the electrons are further excited by the probe pulse to higher energy states after the pump excitation.

From the TR spectra, the excited state dynamics can be probed by examining the kinetic trace of the probe wavelength. From Fig. 2, the strong PB signal at 560-nm probe has a transient signal that lasted tens of ps. Comparing to 525-nm probe that decays within a few ps, the slow decay corresponds to additional relaxation channel that is absent at 525-nm probe which will be further discussed. Therefore, probing at 560 nm should give additional dynamics not present at 525-nm probe. The PB signal can be understood as the occupation of excited state due to pump excitation as depicted by the solid circles in Fig. 3. The absorption of the probe light is reduced as the higher energy states are occupied that increases the transient reflectivity, giving the PB signal. To obtain the relaxation time of the excited state, the kinetic trace is fitted with exponential decay. From the TR spectra, we found out that the 560-nm probe can be fitted with bi-exponential decay while the 525-nm probe can be fitted with mono-exponential decay. The result of the bi-

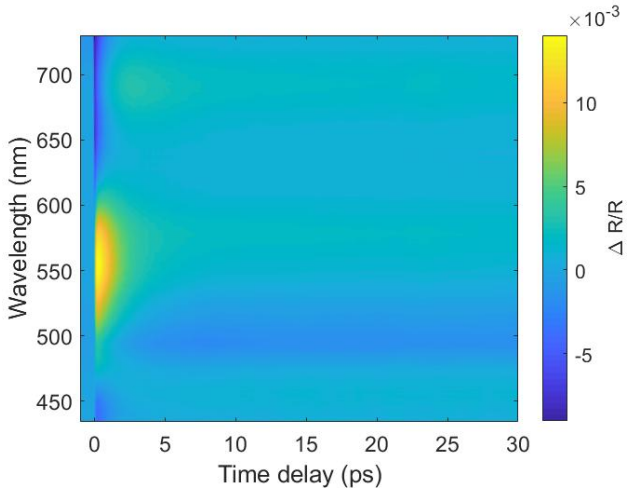

FIG. 2. Pseudo-color TR spectra plot for TaAs excited by 800 nm pump with pump fluence of 480 μJ/cm^2.

exponential decay fitting is a fast (τ_{fast} = 1.55±0.01 ps) and a slow (τ_{slow} = 190±10 ps) decay component as depicted in Fig. 4(a). The mono-exponential decay gives a fast (τ_{fast} = 1.59±0.01 ps) decay component, as depicted in Fig. 4(b), which is comparable to the fast relaxation obtained previously using 560-nm probe. This suggests that the single relaxation channel at 525-nm probe share the same mechanism as the fast relaxation observed for 560-nm probe.

To understand the origin of the fast decay, we compare the transient dynamics with traditional semimetal bismuth (Bi). For Bi, the conduction and valence band extrema are at different k-points, so e-h recombination is mediated by phonons [36]. The e-h recombination dynamics in Bi has been reported to be in the few ps range from two-dimensional optical-pump terahertz-probe [37] and optical-pump optical-probe [36] measurements. This establishes the upper limit of the e-h recombination time in TaAs since, in TaAs, e-h recombination does not require the mediation by phonons as the conduction and valence band overlaps at the same k-point. Also, the timescale of the fast decay is consistent with e-h recombination in TaAs reported in literature by transient grating measurement [34] which is sensitive to density of photoexcited carriers. Furthermore, this timescale is also similar to reported recombination time (∼1 ps) in graphene [38, 39] which has similar gapless dispersion as TaAs. Therefore, we ascribe the fast decay component τ_{fast} = 1.55±0.01 ps to e-h recombination as depicted by τ_{e-h} in Fig. 3.

The slow component which decays in few tens of ps could be due to either e-ph coupling or Auger recombination (AR) which occurs on a similar timescale [40, 41]. In e-ph coupling, electrons in higher excited states relax through the emission of phonons. AR is a non-radiative process involving three carriers where energy released by a pair of electron and hole recombination is absorbed by either an electron or hole which is subsequently excited to a higher energy state. To understand the origin of this slower relaxation, we performed TR spectroscopy at different pump fluences. The kinetics at 560 nm under different pump fluence is shown in Fig. 5(a). Fitting the kinetic traces under different pump fluences, the fast and slow relaxation time obtained are shown in Fig. 5(b). From Fig. 5(b) it is clear that both the fast and slow relaxation time increases with increasing pump fluence corresponding to higher initial carrier density. In AR, the relaxation time should *decrease* with increasing carrier population, since more carriers are able to participate in the relaxation process. However, our data shows an opposite trend, suggesting that it is not due to AR. In e-ph coupling on the other hand, the small density of states (DOS) near $E = 0$ [34] limits the carriers relaxing past these states. As the photocarrier population increase with increasing pump fluence, the relaxation time increases as more carriers are required to scatter past these states with small DOS. Therefore, the relaxation time should *increase* with increasing carrier population [40]. Therefore, the fluence-dependent data suggests that the slower relaxation is due to e-ph coupling. The timescale of e-ph coupling observed is much slower compared to that in a semiconductor which is typically few ps [42]. We note that in semiconductor with wide bandgap, the recombination time is very long. This slower relaxation in TaAs could be explained [28] by the reduced DOS near $E = 0$ — during relaxation, the carriers have to scatter past these states with small DOS before relaxing to the lower energy states. However, the small DOS restrict the number of carriers that can scatter to the low energy states thus forming a bottleneck to the relaxation process. This phenomenon is not observed in a semiconductor since relaxation is through intraband transition where such bottleneck is not present.

We obtained two relaxation timescales (τ_{fast} and τ_{slow}) from the fitting result of the 560-nm probe while a single relaxation timescale (τ_{fast}) from the 525-nm probe. We attribute the fast decay component to e-h recombination, and the slow decay to e-ph coupling. The absence of the slow decay component at 525-nm probe will be further discussed in the following section.

IV. DISCUSSION

A. Dual relaxation channels in TaAs

The fluence-dependent data suggests that the hot-electron dynamics is similar to that of semiconductors. The optical pump pulse excites the electrons far above the Weyl nodes into a non-thermal distribution. These electrons subsequently undergo momentum randomization [43] and thermalization via electron-electron scattering in the tens of femtosecond timescale [34], resulting in the electron and hole distribution following a Fermi-Dirac distribution $f_e(E)$ and $f_h(E)$ respectively over all

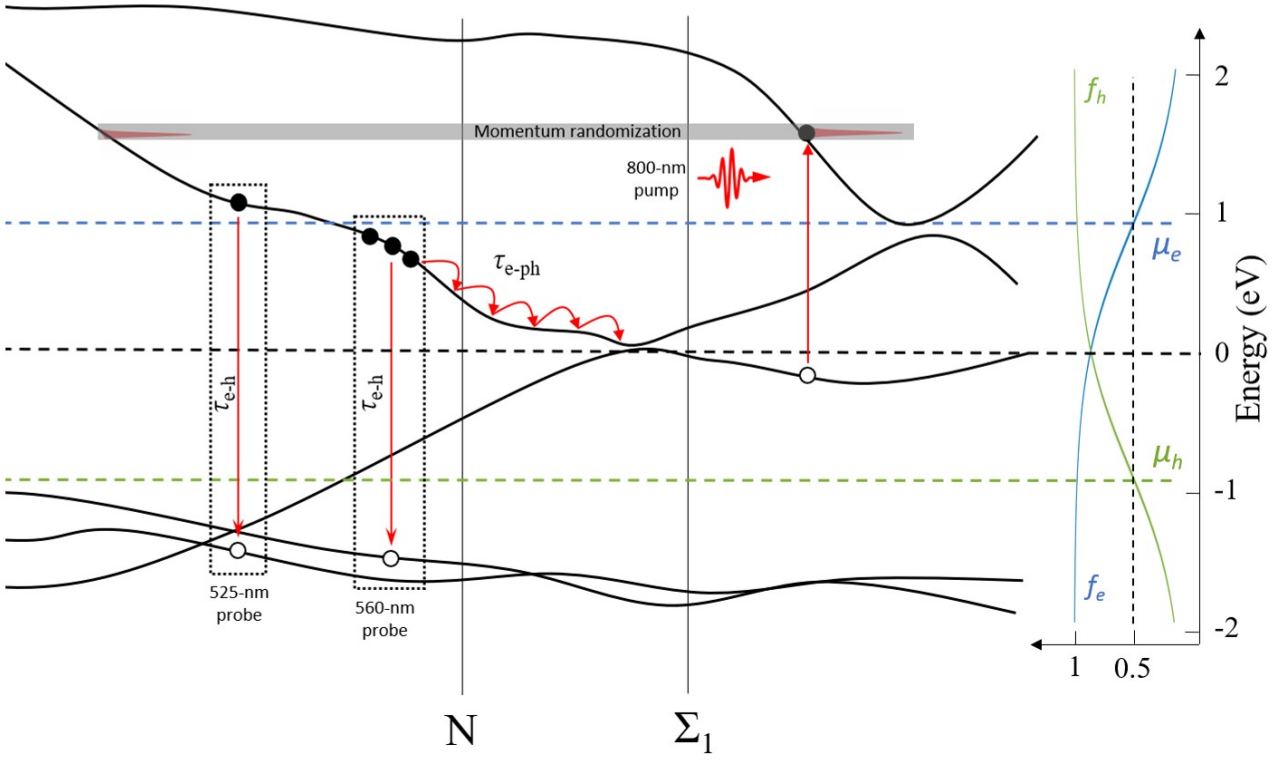

FIG. 3. Realistic band structure schematic of TaAs calculated with density functional theory using the Perdew-Burke-Ernzerhof exchange-correlation functional (including spin-orbit coupling) [28], depicting the asymmetric populations of electrons (solid circles) and holes (hollow circles) after thermalization. The dotted boxes indicate the regions corresponding to the 525 and 560 nm absorption.

allowed k-vectors in the entire Brillouin zone. These electrons in excited states then relax to the ground state through e-h recombination. This transition corresponds to τ_{e-h} which we observed in our experiment as illustrated in Fig. 3. This physical picture although has been able to explain the carrier dynamics in various material like semiconductor [38] and perovskites [40], does not provide an explanation for dual relaxation in TaAs. It does not provide an explanation for the electron relaxation via a second, slower relaxation channel instead of just following the faster and more efficient relaxation channel. This problem can be explained by looking at the carrier population immediately after thermalization, which can be deduced indirectly from the steady-state absorption spectra. The absorption spectra tells us the joint density of states (JDOS) for different probe wavelengths — a higher JDOS corresponds to a wider range of k-vectors where optical transitions are possible, as depicted by the wider dotted box on the left portion of Fig. 3. Hence a higher JDOS corresponds to more available excited states for the electrons to scatter to during thermalization. In addition, the chemical potential of electrons (μ_e) and holes (μ_h) after thermalization are at different energies which is estimated from $N_{e/h} = \int_0^\infty dE f_{e/h}(E) g_{e/h}(E)$ where $g_{e/h}(E)$ is the DOS in the conduction/valence band for electron/hole, in the parabolic-band approximation. From the Fermi-Dirac function, we see that states below μ_e are filled with electrons while states above μ_h are filled with holes. Hence, the occupation factor of *holes* below μ_h is small, implying low concentration of holes in these states. This results in an asymmetric population of electrons and holes as depicted in Fig. 3. Recombination of the excited electrons to the lower-energy hole states are thus limited by the low hole concentration at these states. Therefore, the remaining excited-state electrons can only relax via other channels.

Besides comparing the fast decay timescale to the reported recombination time in semimetals, we further verify that the fast decay corresponds to recombination by comparing the fluence-dependent results with literature. Since the band structure of graphene is similar to those in Weyl semimetals, the fluence dependence of the relaxation times should be similar to that of TaAs. The recombination time in graphene has been reported to exhibit a positive correlation with carrier density [39], consistent with our fluence-dependent τ_{fast} in TaAs as shown in Fig. 5. As the pump fluence increases, more carriers are generated, increasing the carrier density where the recombination time is expected to increase.

At the same time, hot electrons can relax through an

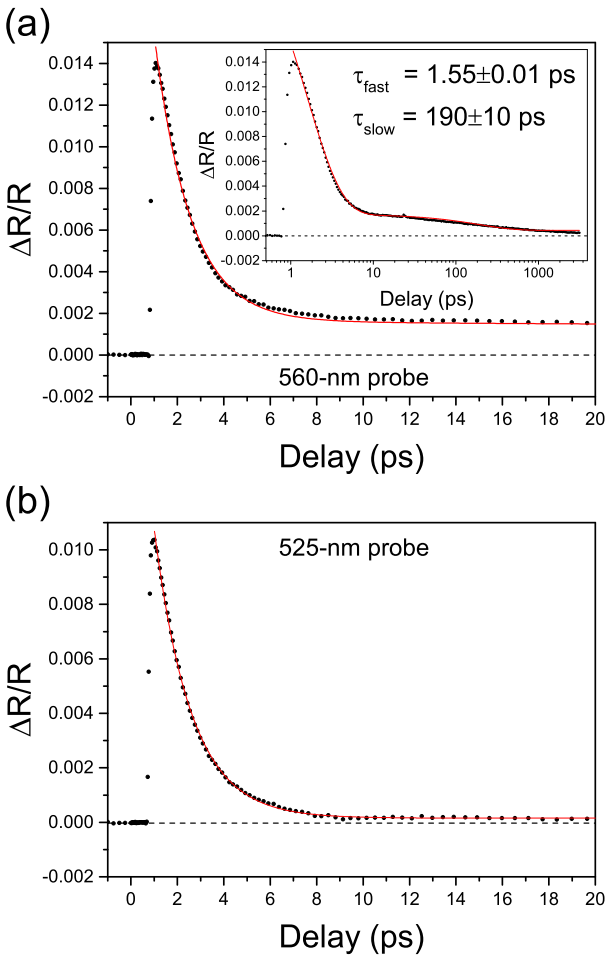

FIG. 4. Experimental data (solid circle) fitted with exponential decay (solid line) for (a) 560-nm probe and (b) 525-nm probe under 480 μJ/cm^2 pump fluence. Dashed line is the data before pump.

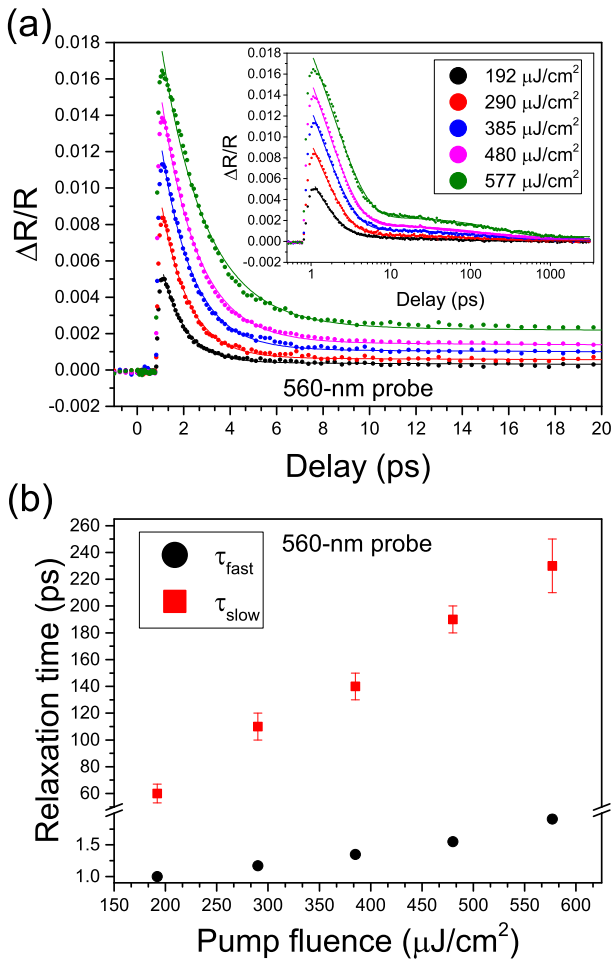

FIG. 5. (a) Experimental data (solid circle) fitted with bi-exponential decay (solid line). Multiple kinetics at 560 nm probe wavelength under different pump fluence. Inset shows kinetics at longer pump probe delay. (b) Relaxation time under different pump fluence.

additional relaxation channel, namely carrier cooling via e-ph coupling as denoted by τ_{e-ph} in Fig. 3. This relaxation mechanism is slower than the recombination lifetime due to the following reasons. Firstly, the photoexcited electrons are required to scatter past the $E = 0$ states (near Σ_1 in Fig. 3) before relaxing to the lower-energy states [34]. However, the small DOS limits this relaxation process and thus increases the relaxation time. Secondly, the relaxation to different k-points via e-ph coupling require the emission of phonons. However, these electrons can subsequently reabsorb the phonons, thus slowing down the electron cooling process [40]. This explanation is consistent with our pump fluence data in Fig. 5(b). As the pump fluence increases, the density of the photoexcited hot carriers increases, which during relaxation, emits a larger number of phonons, which in turn increases the reabsorption of phonons by the carriers, that ultimately increases the relaxation time τ_{slow}. Since e-h recombination does not require scattering past states with low DOS nor phonon emission, e-h recombination can be more efficient than e-ph coupling in TaAs. Therefore, the combination of small DOS and phonon reabsorption by the carriers make e-ph coupling an inefficient relaxation mechanism compared to e-h recombination.

B. Quenching of electron-phonon coupling

From the steady-state absorption spectrum in Fig. 1, we see that starting at 475 nm, absorption increases with increasing wavelength and peaks at 560 nm. Above a certain absorption threshold (∼2.51 in Fig. 1) corresponding to probe wavelength longer than ∼525 nm, there is a larger JDOS between the initial and final states. The majority of the photoexcited electrons thus thermalize and occupy regions in k-space corresponding to these "final" states (from steady-state absorption data) with large JDOS, then start their cooling process either by

the dual channels of e-h recombination and e-ph coupling. On the other hand, the JDOS is smaller for probe wavelength shorter than ∼525 nm. This corresponds to regions of k-space where there are fewer thermalized hot electrons, and so the electrons should be able to relax entirely through the more efficient e-h recombination as depicted schematically by the narrower dotted box in Fig. 3. This picture is consistent with our experimental observation of a single-exponential relaxation for probe wavelengths shorter than 525 nm, and double-exponential relaxation for probe wavelength longer than 525 nm. Interestingly, we can see that for probe wavelength longer than 525 nm, there is a very long-lived (∼ns) constant offset, which may be related to carriers that have already relaxed to the Dirac point — there the vanishingly small DOS makes further relaxation extremely inefficient. The kinetics at 525-nm probe can be fitted well with a mono-exponential decay, shown in Fig. 4(b), with a relaxation time of (1.59±0.01) ps. Also, absence of the slow decay due to e-h coupling at 525-nm probe is consistent with our physical model described above.

From classical electrodynamics, the current density is proportional to the carrier density of the photogenerated electrons/holes in the conduction/valence band. However, how long such photoinduced current can be sustained depends on how fast these photocarriers relax or recombine [44, 45]. In our study we found that the carrier dynamics in TaAs contains an extremely slow component, which could provide an explanation of the large time-integrated photocurrent reported in literature [24].

V. CONCLUSION

In summary, we have performed TR spectroscopy on TaAs where the electrons are excited by the 800 nm pump pulse. In our experiment, we observed a fast (∼1ps) and slow relaxation (∼190ps) in TaAs when probing at 560 nm. The timescale of the relaxation is consistent with mechanism reported in literature for TaAs [34]. The origin of this slow relaxation component is attributed to the small DOS near $E = 0$ and phonon reabsorption during carrier cooling. The fast and slow decay component corresponds to e-h recombination and e-ph coupling respectively. Also, the relaxation time of both channels increase with increasing pump fluence due to high carrier density. Furthermore, we found that by changing the probing wavelength, from 560 nm to 525 nm, relaxation through e-ph coupling is not observable. This quenching of e-ph relaxation channel is due to fewer electrons in the corresponding excited state immediately after thermalization, which allows all the carriers to relax through the more-efficient e-h recombination channel. An understanding of the carrier dynamics of TaAs might pave the way for the application in sensitive optoelectronics.

ACKNOWLEDGMENTS

We acknowledge funding from the Singapore Ministry of Education (MOE) AcRF Tier 1 (MOE2018-T1-1-097 & RG95/19 (S)) and A*STAR PHAROS Programme on 2D Materials (SERC Grant No. 152 70 00016). Work at Los Alamos was carried out under the auspices of the U.S. Department of Energy (DOE) National Nuclear Security Administration under Contract No. 89233218CNA000001 and was supported by LANL LDRD Program. It was supported in part by Center for Integrated Nanotechnologies, a DOE BES user facility.

[1] M. Z. Hasan and C. L. Kane, Rev. Mod. Phys. **82**, 3045 (2010).
[2] L. Fu, C. L. Kane, and E. J. Mele, Phys. Rev. Lett. **98**, 106803 (2007).
[3] S. Cai, J. Guo, V. A. Sidorov, Y. Zhou, H. Wang, G. Lin, X. Li, Y. Li, K. Yang, A. Li, *et al.*, npj Quantum Mater. **3**, 62 (2018).
[4] X. Zhang, J. Wang, and S.-C. Zhang, Phys. Rev. B **82**, 245107 (2010).
[5] J. Yao, J. Shao, Y. Wang, Z. Zhao, and G. Yang, Nanoscale **7**, 12535 (2015).
[6] H. Zhang, X. Zhang, C. Liu, S.-T. Lee, and J. Jie, ACS Nano **10**, 5113 (2016).
[7] Y. Huang, Y. Song, S. Wang, I. Buyanova, and W. Chen, Nat. Commun. **8**, 15401 (2017).
[8] K. Vaklinova, A. Hoyer, M. Burghard, and K. Kern, Nano Lett. **16**, 2595 (2016).
[9] S. M. Hus, X.-G. Zhang, G. D. Nguyen, W. Ko, A. P. Baddorf, Y. P. Chen, and A.-P. Li, Phys. Rev. Lett. **119**, 137202 (2017).
[10] A. Dankert, J. Geurs, M. V. Kamalakar, S. Charpentier, and S. P. Dash, Nano Lett. **15**, 7976 (2015).
[11] Z. Wang, Y. Sun, X.-Q. Chen, C. Franchini, G. Xu, H. Weng, X. Dai, and Z. Fang, Phys. Rev. B **85**, 195320 (2012).
[12] Z. Liu, J. Jiang, B. Zhou, Z. Wang, Y. Zhang, H. Weng, D. Prabhakaran, S. Mo, H. Peng, P. Dudin, *et al.*, Nat. Mater. **13**, 677 (2014).
[13] H. Yi, Z. Wang, C. Chen, Y. Shi, Y. Feng, A. Liang, Z. Xie, S. He, J. He, Y. Peng, *et al.*, Sci. Rep. **4**, 6106 (2014).
[14] S. M. Young, S. Zaheer, J. C. Teo, C. L. Kane, E. J. Mele, and A. M. Rappe, Phys. Rev. Lett. **108**, 140405 (2012).
[15] B.-J. Yang and N. Nagaosa, Nat. Commun. **5**, 4898 (2014).
[16] A. Zyuzin, S. Wu, and A. Burkov, Phys. Rev. B **85**, 165110 (2012).
[17] R. Wang, J. Zhao, Y. Jin, W. Xu, L.-Y. Gan, X. Wu, H. Xu, and S. Tong, Phys. Rev. B **96**, 121104 (2017).

[18] S.-Y. Xu, I. Belopolski, N. Alidoust, M. Neupane, G. Bian, C. Zhang, R. Sankar, G. Chang, Z. Yuan, C.-C. Lee, *et al.*, Science **349**, 613 (2015).

[19] G. Resta, S.-T. Pi, X. Wan, and S. Y. Savrasov, Phys. Rev. B **97**, 085142 (2018).

[20] X. Huang, L. Zhao, Y. Long, P. Wang, D. Chen, Z. Yang, H. Liang, M. Xue, H. Weng, Z. Fang, *et al.*, Phys. Rev. X **5**, 031023 (2015).

[21] H. Weng, R. Yu, X. Hu, X. Dai, and Z. Fang, Adv. Phys. **64**, 227 (2015).

[22] Q. Ma, S.-Y. Xu, C.-K. Chan, C.-L. Zhang, G. Chang, Y. Lin, W. Xie, T. Palacios, H. Lin, S. Jia, *et al.*, Nat. Phys. **13**, 842 (2017).

[23] S. Kimura, Y. Nakajima, Z. Mita, R. Jha, R. Higashinaka, T. D. Matsuda, and Y. Aoki, Phys. Rev. B **99**, 195203 (2019).

[24] S. Chi, Z. Li, Y. Xie, Y. Zhao, Z. Wang, L. Li, H. Yu, G. Wang, H. Weng, H. Zhang, *et al.*, Adv. Mater. **30**, 1801372 (2018).

[25] S. Patankar, N. Nair, J. Analytis, J. Orenstein, and L. Wu, in *Proc. SPIE*, Vol. 10530 (2018) p. 1053003.

[26] L. Wu, S. Patankar, T. Morimoto, N. L. Nair, E. Thewalt, A. Little, J. G. Analytis, J. E. Moore, and J. Orenstein, Nat. Phys. **13**, 350 (2017).

[27] K. Sun, S.-S. Sun, L.-L. Wei, C. Guo, H.-F. Tian, G.-F. Chen, H.-X. Yang, and J.-Q. Li, Chin. Phys. Lett. **34**, 117203 (2017).

[28] J. Buckeridge, D. Jevdokimovs, C. Catlow, and A. Sokol, Phys. Rev. B **93**, 125205 (2016).

[29] C. Zhang, C. Guo, H. Lu, X. Zhang, Z. Yuan, Z. Lin, J. Wang, and S. Jia, Phys. Rev. B **92**, 041203 (2015).

[30] I. Song, C. Park, and H. C. Choi, RSC Adv. **5**, 7495 (2015).

[31] Appl. Phys. Express **2**, 025003 (2009).

[32] A. Rawat, N. Jena, A. De Sarkar, *et al.*, J. Mater. Chem. A **6**, 8693 (2018).

[33] N. Sirica, Y. Dai, L. Zhao, G. Chen, B. Xu, R. Yang, B. Shen, N. Ni, D. Yarotski, S. Trugman, *et al.*, in *Conference on Lasers and Electro-Optics (CLEO)* (Optical Society of America, 2018).

[34] C. P. Weber, B. S. Berggren, M. G. Masten, T. C. Ogloza, S. Deckoff-Jones, J. Madéo, M. K. Man, K. M. Dani, L. Zhao, G. Chen, *et al.*, J. Appl. Phys **122**, 223102 (2017).

[35] Z. Li, H. Chen, S. Jin, D. Gan, W. Wang, L. Guo, and X. Chen, Cryst. Growth Des **16**, 1172 (2016).

[36] Y. Sheu, Y. Chien, C. Uher, S. Fahy, and D. Reis, Phys. Rev. B **87**, 075429 (2013).

[37] I. Timrov, T. Kampfrath, J. Faure, N. Vast, C. Ast, C. Frischkorn, M. Wolf, P. Gava, and L. Perfetti, Phys. Rev. B **85**, 155139 (2012).

[38] J. M. Dawlaty, S. Shivaraman, M. Chandrashekhar, F. Rana, and M. G. Spencer, Appl. Phys. Lett **92**, 042116 (2008).

[39] P. A. George, J. Strait, J. Dawlaty, S. Shivaraman, M. Chandrashekhar, F. Rana, and M. G. Spencer, Nano Lett. **8**, 4248 (2008).

[40] J. Fu, Q. Xu, G. Han, B. Wu, C. H. A. Huan, M. L. Leek, and T. C. Sum, Nat. Commun. **8**, 1300 (2017).

[41] J. Kim, J. Oh, C. In, Y.-S. Lee, T. B. Norris, S. C. Jun, and H. Choi, ACS Nano **8**, 2486 (2014).

[42] X.-C. Nie, H.-Y. Liu, X. Zhang, C.-Y. Jiang, S.-Z. Zhao, Q.-P. Zhao, F. Li, L. Yue, J.-Q. Meng, Y.-X. Duan, *et al.*, Results Phys **12**, 1089 (2019).

[43] A. Othonos, J. Appl. Phys **83**, 1789 (1998).

[44] B. M. Fregoso, Phys. Rev. B **100**, 064301 (2019).

[45] E. Vella, H. Li, P. Grégoire, S. M. Tuladhar, M. S. Vezie, S. Few, C. M. Bazán, J. Nelson, C. Silva-Acuña, and E. R. Bittner, Sci. Rep **6**, 29437 (2016).